J. Fluid Mech. (1992), *vol.* 245, *pp.* 669–699

Swirling flow in an axisymmetric cavity of arbitrary profile, driven by a rotating magnetic field

By P. A. DAVIDSON

Department of Mechanical Engineering, Imperial College of Science and Technology, Exhibition Road, London SW7 2BX, UK

(Received 28 August 1991 and in revised form 10 July 1992)

We investigate the swirling flow of liquid metal in an axisymmetric cavity of arbitrary profile, generated by a rotating magnetic field. In addition to the primary swirling motion, a recirculation is generated by the Bödewadt-like boundary layers on the inclined sides of the cavity. As in the classic problem of 'spin-up' in a cylinder, this secondary flow has a dominating effect over the distribution of angular momentum. It is shown that, in the inviscid core, the angular momentum is independent of z, the axial coordinate, and that the applied body force is balanced by the Coriolis force. The bulk of the streamlines pass through both the core and the boundary layer, picking up energy in one region and losing it in the other. By matching the angular momentum and recirculating mass flux in the core to that in the boundary layer, a single governing equation is established for the swirl distribution. This second-order ordinary differential equation is valid for any axisymmetric shape, but is solved here for two cases; those of flow in a truncated cylinder and in a hemisphere. The former of these is compared with previously published experimental data, and with a full numerical simulation. Finally, we extend some of these ideas to buoyancy-driven flow. Here we take advantage of the analogy between centrifugal and thermally stratified flows to model natural convection of liquid metal in a cavity.

1. Introduction

Suppose that a uniform, transverse magnetic field, $\boldsymbol{B}$, permeates an axisymmetric cavity, and is rotated about the vertical axis of symmetry. (This is shown schematically in figure 1.) Now suppose the cavity is filled with liquid metal. At the most elementary level, we may regard the liquid as constituting the rotor of an induction motor, and so it is clear that the liquid will itself rotate, following the motion of the magnetic field. However, we shall see that, in addition to this swirling motion, a strong secondary flow is created. This flow is generated by the cavity boundaries, and dominates the behaviour of the liquid metal.

There have been a considerable number of studies of magnetically induced swirl in cavities of varying shapes, each motivated by a particular industrial process. The literature is exhaustive and we shall only mention a few typical examples. Zibol'd *et al.* (1986) were concerned with swirl in a cylindrical cavity, in the context of single crystal growing. This problem is complicated by rotation of the walls, and they investigated the flow numerically. Boyarevich & Millere (1982) considered swirl in a hemisphere, driven by a static electric current and magnetic field. The motivation for this work stemmed from electric-arc welding. In addition to an azimuthal body force, which induces swirl, there was a poloidal component of force, creating motion in the

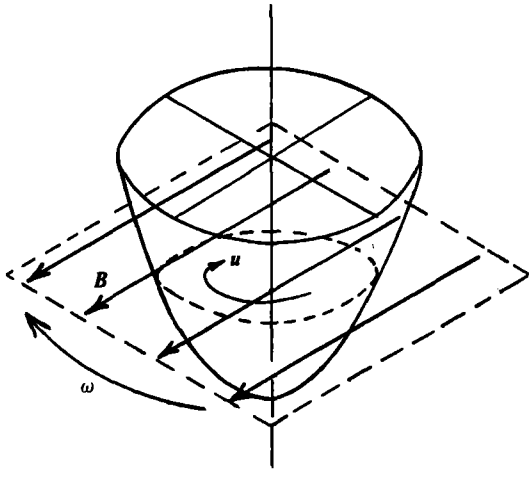

FIGURE 1. The geometry under consideration. An axisymmetric cavity is filled with liquid metal and subjected to a rotating magnetic field.

(r, z)-plane. As in the paper mentioned first, the study consisted essentially of (laminar) numerical experiments at low Reynolds number. Swirl in a parabolic cavity was studied by Vlasyuk & Sharamkin (1987), motivated this time by electric-arc remelting of ingots. As in Boyarevich & Millere's work, flow was induced by both poloidal and azimuthal body forces, generated by d.c. fields. Again, the study was numerical in nature, and restricted to low Reynolds numbers. The same problem was also tackled by several authors in a cylindrical geometry. Typical of these studies is the work of Muizhnieks & Yakovich (1988).

These investigations are complemented by a number of laboratory experiments. Perhaps the most comprehensive is that of Robinson (1973), who applied an (almost) purely azimuthal force to mercury in a truncated cylinder. We shall return to this paper later. A similar study was undertaken by Doronin, Dremov & Kapusta (1973). Finally, Vives & Perry (1988) looked at both natural and (magnetically) forced convection in a cylinder, and its influence on solidification.

One of the aims of this paper is to provide a unified theoretical framework, within which these different studies may be assessed. As with Vives & Perry (1986), the original motivation for this work lay in the use of rotary electromagnetic stirring in the casting industry. A simple representation of an aluminium caster is given in figure 2. In essence, a solid ingot is slowly withdrawn from a liquid-metal pool, the pool being continuously replenished from above. During solidification, alloying elements tend to segregate out from the host metal, giving rise to inhomogeneity in the final ingot. One means of homogenizing the melt as it solidifies is to stir the liquid using a rotating, horizontal magnetic field. This practice is widespread in the steel industry, and can also be applied to the casting of aluminium, or indeed any other metal. (Rotary electromagnetic stirring, as defined here, should not be confused with the electromagnetic casting of aluminium, in which a vertical magnetic field is used to support the sides of the liquid pool, obviating the need for a mould.)

In the case of a steel caster, the liquid metal pool is essentially a long deep cone, perhaps 0.3 m wide and 10 m long. Rotary magnetic stirring has been studied in this context by, amongst others, Davidson & Hunt (1987). In that study, the pool was treated as an infinitely long liquid-metal column. One important consequence of the

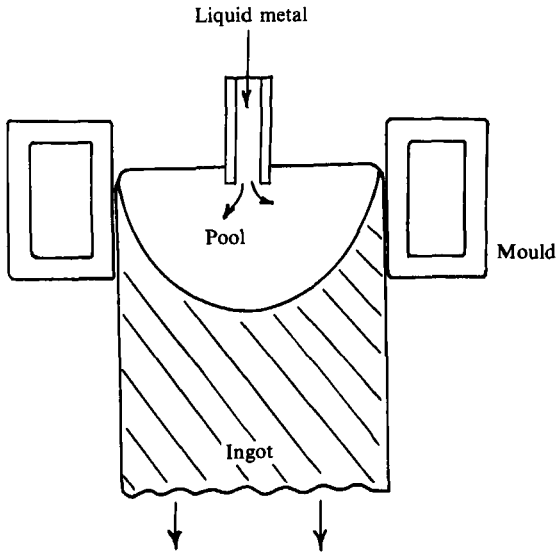

FIGURE 2. Casting of aluminium.

great depth of the pool is that the flow is geometrically unconfined in the axial direction.

In the casting of aluminium, the pool is more hemispherical in shape, and so boundaries are inclined to the axis of rotation. It is this second geometry which is the subject of the present paper. We shall show that the geometrical confinement of the flow plays a key role in the dynamics.

In the case of a steel caster, the induced swirl chooses an axial lengthscale (i.e. axial penetration of the flow) which far exceeds the axial extent of the applied magnetic body force. It is through the choice of this lengthscale that the fluid establishes its equilibrium (Davidson & Hunt 1987). This is achieved when the boundary layers on the solid cylindrical surface have sufficient axial length for the dissipation of energy within these layers to counter the energy imparted to the fluid by the body force. However, such an undetermined lengthscale is not available to our geometrically confined flow.

We may generalize this argument as follows. Let $\boldsymbol{F}$ be the time-averaged component of the Lorentz body force, $\boldsymbol{u}$ be the induced velocity, and ν be the viscosity of the liquid metal. We shall consider the net energy balance in a forced, laminar flow (although the arguments are readily extended to turbulent flows). Integrating the Navier–Stokes equation around any streamline which is closed in the (r,z)-plane, we find,

$$\oint \boldsymbol{F}\cdot \mathrm{d}\boldsymbol{r} + \nu \oint \nabla^2 \boldsymbol{u}\cdot \mathrm{d}\boldsymbol{r} = 0. \tag{1}$$

This states that the energy gained by a fluid particle, by virtue of the work done by $\boldsymbol{F}$, must be diffused and dissipated out of the particle by shear. However, the Reynolds number for these flows is invariably large ($Re > 10^5$), so we might expect the second integral to be small. As Mestel (1989) pointed out, there are several ways that (1) could be realized: (*a*) the streamlines align themselves such that $\oint \boldsymbol{F}\cdot \mathrm{d}\boldsymbol{l} = 0$; (*b*) $\boldsymbol{u}$ scales as $1/\nu$; (*c*) the streamlines (but not the force) have a characteristic length which scales as $1/\nu$; (*d*) every streamline passes through a singular region such as a viscous boundary layer.

It seems implausible that condition (*a*) could be satisfied in the present context,

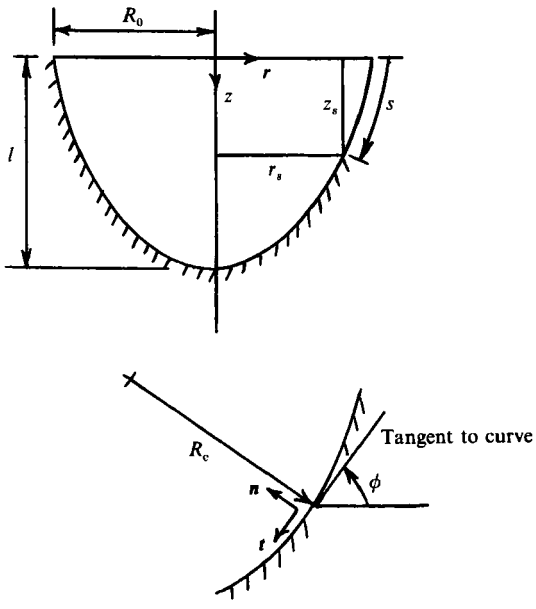

FIGURE 3. Coordinate system.

and we shall not consider this further. Mestel (1989) was particularly concerned with flows of type (*b*), induced by a rotating field in two-dimensional and axisymmetric geometries. One example of a flow of type (*c*) is the rotary stirring of steel. For the flow shown in figure 1, there is no undetermined global lengthscale available to the fluid, and (1) must be satisfied by either option (*b*) or option (*d*). It is the premise of this paper that the flow defined in figure 1 is of type (*d*). That is, it is the boundary layers which have the controlling influence on the flow, rather than dissipation in the core. Clearly, this leads to a much lower velocity than that associated with option (*b*).

The physical mechanism by which the boundary layers control the flow may be explained by reference to a simpler, well-known phenomenon. Consider the text-book problem of 'spin-down' of a stirred cup of tea. In this example, the main body of the fluid is predominantly in a state of inviscid rotation. The centrifugal force is balanced by a radial pressure gradient, and this radial pressure gradient is also imposed throughout the boundary layer on the bottom of the cup. However, the angular momentum of the fluid in the boundary layer is smaller than that of the core, and so there is a local imbalance between the imposed pressure gradient and centripetal acceleration. The result is a radial inflow, with the fluid eventually drifting up and out of the boundary layer. As each fluid particle passes through the boundary layer, it gives up a significant fraction of its kinetic energy. The tea finally comes to rest when all the contents of the cup have been flushed through the boundary layer. We shall see that a similar process occurs in our forced, swirling flow.

We shall employ a cylindrical polar coordinate system (r, θ, z), as shown in figure 3. In addition, it is convenient to introduce a curvilinear coordinate, s, measured along the surface, and an angle, ϕ, giving the local inclination of the boundary to the horizontal. The coordinates of the boundary are given by (r_s, z_s), and the unit normal and tangential vectors to the surface are $\boldsymbol{n}$ and $\boldsymbol{t}$. Let the maximum radius and depth of the pool be R_0 and l respectively, and R_c be the local radius of curvature of the surface.

We shall assume that the surface of the liquid metal remains flat, and acts, in

effect, as a plane of symmetry. In addition, we shall ignore the complications introduced in a caster, such as withdrawal of the ingot, flow into the top surface of the pool, and solidification at the boundaries. It follows from these simplifications that the theory presented here is also applicable to motion in an axisymmetric, closed container, such as a sphere or ellipsoid.

Electrically, we shall assume that a return path is provided for any eddy currents, J, which impinge on the surface of the cavity. Formally, we shall treat the surface as a plane of symmetry, where the vertical gradients in J are zero. In principle, it would not be difficult to extend the analysis to cases where the surface is electrically insulated, or where it is curved. In the former case, we would simply have to modify the specified body force distribution. However, in the interests of simplicity, we shall restrict ourselves to the simpler boundary condition.

In §2, we shall consider the distribution of the electromagnetic body force. The remainder of the paper is concerned with the hydrodynamic consequences of this force. However, before proceeding to solve the general case, defined by figure 1, it is useful to consider a much simpler problem: that of forced swirling flow between infinite parallel discs. This simpler flow exhibits many of the key features of the more general problem, and so it is discussed in some detail in §3. Next, in §§4–9, we address the problem of forced swirl in an arbitrary axisymmetric cavity, dealing first with the interior (core) flow, and then with the boundary layers. Most of the discussion will centre on turbulent flow, partly because laboratory experiments fall into this regime, and partly because the laminar flow is likely to be unstable for all but low Reynolds numbers. To illustrate the general theory, the specific cases of flow in a flat-bottomed cavity and flow in a hemisphere are discussed in §§10 and 11.

Finally, there is a well-known analogy between swirling flow and buoyancy-driven flow, the latter being of considerable practical importance in the casting of aluminium. In §12, we shall show briefly that some of the ideas developed for forced swirl are also applicable to buoyancy-driven flow in a cavity.

2. The time-averaged magnetic body force

The rotating magnetic field induces both a time-averaged, and an oscillatory component of force in the liquid metal. Generally, the inertia of the fluid is sufficiently large for the oscillatory component to be ignored, i.e. $\sigma B^2/\rho\omega \ll 1$. (See Davidson & Hunt 1987.) To calculate the time-averaged body force, we shall assume that the cavity is housed at the top of a solid metal column, composed of the same metal as the pool, as shown in figure 2.

Provided the motion of the liquid metal is not too great, the magnetic field remains unperturbed by the swirl induced in the melt. The body force may then be calculated on the assumption that the melt acts as a stationary, solid conductor. Formally, we must ensure that the magnetic Reynolds number, $uR_0\mu\sigma$, is small. (Here, μ is the permeability of free space, and σ is the electrical conductivity of the metal.) This condition is usually satisfied in industrial applications (Davidson & Hunt 1987) and we shall make this approximation here.

For simplicity, we shall make one further approximation. We shall limit ourselves to low-frequency magnetic fields. Specifically, we shall choose the field frequency, ω, to satisfy

$$\omega R_0^2 \mu\sigma \leqslant 3.$$

Under this condition, the time-averaged body force may be estimated on the assumption that the applied magnetic field is unperturbed by the presence of the

conducting column. To within a 4% error, the force is then given by the low-frequency result

$$F_\theta = \tfrac{1}{2}B^2\sigma\omega r \tag{2}$$

(See Dahlberg 1972 and Davidson & Hunt 1987.) Here the subscript θ indicates that the body force is purely azimuthal.

From a theoretical point of view, there is no particular reason why we should limit ourselves to such low frequencies. The theory presented here is readily extended to fields which do not satisfy the inequality above. The motivation for this simplification is merely that (2) gives us a particularly simple 'model' body force. It also happens that many of the experiments which have been performed, with which we shall compare our theory, satisfy this restriction.

With an eye to the inertial force in the Navier–Stokes equation, we shall rewrite (2) in the form

$$F_\theta = \tfrac{1}{2}\rho\Omega_t^2 r, \tag{3}$$

where Ω_t has the dimensions of s^{-1}, and is given by

$$\Omega_t = B(\sigma\omega/\rho)^{\frac{1}{2}}. \tag{4}$$

3. Forced laminar flow between infinite parallel discs

Consider the following problem. Two infinite parallel discs are separated by a distance $2w$, and the gap filled with liquid metal. The body force F_θ is applied to the metal, inducing a laminar swirling recirculating flow. This situation is illustrated in figure 4.

Clearly, this geometry is somewhat different to that shown in figure 1. Nevertheless, a review of this simple, if atypical case forms a useful precursor to the more complex problem of swirl in a cavity. Specifically, flow between infinite discs exhibits many of the key physical features of our more general problem. Moreover, it has a simple analytical solution, and so the details of the flow are particularly accessible.

Some features of this flow have already been discussed by Gorbachev & Nikitin (1973). They were interested in swirl induced by static crossed electric and magnetic fields. However, their body force is essentially the same as ours. Their method of analysis was approximate, involving an averaging of the inertial terms across the boundary layer. Unfortunately, as we shall see, their analysis contains one fundamental mistake.

Note that, in figure 4, we have shown a radially inward flow in the boundary layers. Fluid enters the boundary layers at infinity, flows towards the axis, and then, in order to satisfy continuity, gradually drifts out into the core. As explained in the introduction, this radial flow at the disc surface is driven by a local imbalance between the centripetal acceleration and the imposed, radial pressure gradient. A formal example of this type of flow is Bödewadt's problem of rotating fluid over an infinite, stationary disc. (See, for example, Greenspan 1968.)

Consider the flow in the lower half of the gap, $0 \leqslant z \leqslant w$, shown in figure 4. We shall look for a solution in the form of the von Kármán similarity variables. That is, we let the velocity components have the form

$$u_r = \Omega r F(z/l), \quad u_\theta = \Omega r\, G(z/l), \quad u_z = \Omega l\, H(z/l), \quad p = \tfrac{1}{2}\rho\Omega^2 r^2 + \rho\Omega^2 l^2 P(z/l).$$

Here p is the pressure, l is a characteristic lengthscale, and Ω is a characteristic rotation rate, which we shall take as the rotation rate in the core of the flow. Away

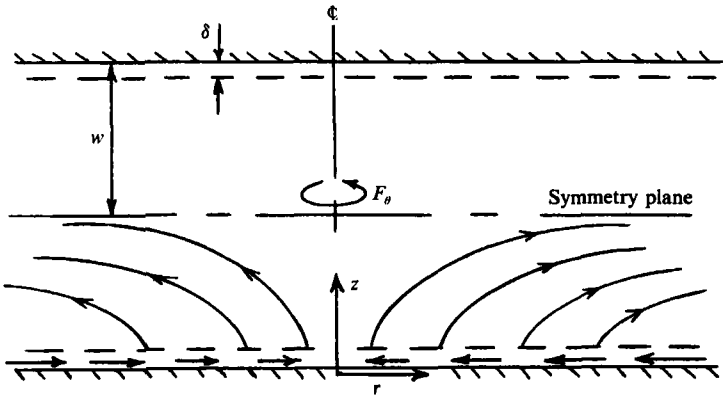

FIGURE 4. Swirling flow between two discs.

from the disc surface, we may take l as equal to the gap width, $l_c = w$, while in the boundary layer, we may take l as the von Kármán boundary-layer thickness, $l_b = (\nu/\Omega)^{\frac{1}{2}}$. The ratio of these lengthscales is

$$\epsilon = (\nu/\Omega)^{\frac{1}{2}}/w = l_b/l_c. \tag{5}$$

We shall take ϵ to be vanishingly small, and employ the method of matched asymptotic expansions to blend the flow in the two regions.

If we substitute the proposed velocity functions into the Navier–Stokes equation

$$\boldsymbol{u}\cdot\nabla\boldsymbol{u} = -\nabla(p/\rho) + \nu\nabla^2\boldsymbol{u} + \boldsymbol{F}_\theta$$

then we obtain three coupled ordinary differential equations valid in both regions:

$$F^2 + HF' - G^2 + 1 = (\nu/\Omega l^2)F'', \tag{6}$$

$$2FG + G'H = (\nu/\Omega l^2)G'' + \tfrac{1}{2}\Omega_f^2/\Omega^2, \tag{7}$$

$$HH' + P' = (\nu/\Omega l^2)H''. \tag{8}$$

In addition, continuity requires

$$H' + 2F = 0. \tag{9}$$

We shall use subscripts c and b to denote solutions in the core and boundary layer respectively. In the core of the flow, where $l = l_c = w$, the governing equations become

$$F_c^2 + H_c F_c' - G_c^2 = -1, \quad 2F_c G_c + G_c' H_c = \tfrac{1}{2}\Omega_f^2/\Omega^2, \quad H_c' + 2F_c = 0,$$

where the boundary conditions on F_c, G_c and H_c are

$$z/l_c = 1: \quad H_c = 0, \quad F_c' = 0, \quad G_c' = 0;$$
$$z/l_c \to 0: \quad H_c = \epsilon H_b(\infty), \quad G_c = 1.$$

Here $H_b(\infty)$ is the value of H furnished by the boundary-layer solution, and the boundary condition on $G_c(0)$ follows from the definition of Ω. Formally,

$$H_b(\infty) = \lim_{z/l_b \to \infty} H_b(z/l_b).$$

We now expand F_c, G_c and H_c in polynomials of ϵ, and substitute these into the governing equations. To leading order in ϵ, the core velocity functions are given by

$$F_c = \tfrac{1}{2}\epsilon H_b(\infty), \quad G_c = 1, \quad H_c = \epsilon H_b(\infty)\{1 - z/w\}.$$

That is, the velocities in the core are

$$u_r = \tfrac{1}{2}\epsilon H_b(\infty)\,\Omega r, \tag{10}$$

$$u_\theta = \Omega r, \tag{11}$$

$$u_z = \epsilon H_b(\infty)\,\Omega\{w - z\}. \tag{12}$$

The core rotation rate is then given by the azimuthal force balance, which may be rearranged to give

$$\Omega = \frac{\Omega_f}{(2H_b(\infty))^{\frac{2}{3}}}\left[\frac{\Omega_f w^2}{\nu}\right]^{\frac{1}{3}}. \tag{13}$$

Clearly, the core flow is uniquely determined to within one constant, $H_b(\infty)$. Note that the magnetic body force is exactly balanced in the core by the Coriolis force $2\Omega u_r$, and that the angular momentum is independent of z. We shall see later that these emerge as features of our more general problem. We now turn to the boundary-layer equations, in order to find $H_b(\infty)$. Near the disc, (7) takes the form,

$$2F_b G_b + G_b' H_b = G_b'' + \tfrac{1}{2}\Omega_f^2/\Omega^2.$$

However, we have already shown that the last term on the right-hand side of the equation is of order ϵ. Consequently, magnetic forcing is negligible in the boundary layer, and the boundary-layer equations simplify to

$$F_b^2 + H_b F_b' - G_b^2 + 1 = F_b'', \quad 2F_b G_b + H_b G_b' = G_b'', \quad H_b' + 2F_b = 0,$$

with boundary conditions

$$z/l_b = 0: \quad F_b = G_b = H_b = 0;$$

$$z/l_b \to \infty: \quad F_b = 0, \quad G_b = 1, \quad H_b = H_b(\infty).$$

But this is simply a specification of Bödewadt's problem of a rotating fluid over a stationary disc. Its solution is well documented (see, for example Greenspan 1968). The undetermined constant for the core flow is

$$H_b(\infty) = 1.349,$$

from which we find

$$\Omega = 0.516\Omega_f[\Omega_f w^2/\nu]^{\frac{1}{3}}. \tag{14}$$

The boundary-layer thickness, defined by the point $u_\theta = 0.99\Omega r$, turns out to be

$$\delta = 8(\nu/\Omega)^{\frac{1}{2}}.$$

To summarize then, forced, swirling flow between two discs has the following features:

(i) the flow field may be divided into a forced, inviscid core, and two viscous, unforced boundary layers;

(ii) all streamlines pass through both regions, collecting energy in one region and losing it in the other;

(iii) in the core, u_θ and u_r are both independent of z;

(iv) the secondary flow in the core is of order $\delta\Omega$;

(v) the applied Lorentz force is exactly balanced in the core by the Coriolis force.

We shall see that all of these features are reproduced in the more complex and general case of swirl in a cavity.

We might note here that this structure of flow field, involving Ekman pumping between a viscous boundary layer and an inviscid rotating core, is also characteristic

of some models of oceanic circulation. As in the case above, all of the streamlines in these geophysical flows pass through both the core and a boundary layer (Pedlosky 1979).

We now return to the approximate analysis of Gorbachev & Nikitin (1973). They deduced the expression

$$\Omega = 2^{-\frac{2}{3}}\Omega_{\mathrm{f}}[\Omega_{\mathrm{f}} w^2/\nu]^{\frac{1}{3}}.$$

The discrepancy between this result and (13) arises from an incorrect application of the moment of momentum theorem. Suppose that we integrate the torque due to the body force throughout the cylinder $0 < z < w, 0 < r < R$. Let this integral be denoted Δ_{f}.

$$\Delta_{\mathrm{f}} = \int_0^w \int_0^R 2\pi r(rF_\theta)\,\mathrm{d}r\,\mathrm{d}z.$$

Then Gorbachev & Nikitin assumed that this is balanced by the shear stress at the disc surface. That is

$$\int_0^R (\tau_{z\theta} r)\,2\pi r\,\mathrm{d}r = \Delta_{\mathrm{f}}.$$

In fact, evaluating $\tau_{z\theta}$ from Bödewadt's solution shows that

$$\int_0^R (\tau_{z\theta} r)\,2\pi r\,\mathrm{d}r = 0.57\Delta_{\mathrm{f}}.$$

This difference is, of course, because there is an imbalance in the inward flux of angular momentum in the boundary layer, and the outward flux in the core. The inward flux of angular momentum is $1.57\Delta_{\mathrm{f}}$, while the outward flow of angular momentum in the core is $2\Delta_{\mathrm{f}}$.

Notice that the analysis given above does not address the stability of the boundary layers. For some range of Reynolds numbers, the Ekman layer may become unstable and separate. In a similar way, the boundary layers which develop on the cavity wall could also separate. However, we will ignore such cases here.

4. Flow in a cavity: the global balance of energy, vorticity and angular momentum

We now consider forced swirl in a cavity of arbitrary shape. Both laminar and turbulent flows will be considered, and we shall assume that the Reynolds number is high enough for shear stresses (either laminar or turbulent) to be significant only near the boundary. Internal shear layers, or other internal regions of intense dissipation, are excluded. Equation (1), or its equivalent for turbulent flow, then implies that all streamlines must pass through the boundary layer, δ, and the flow field is as shown schematically in figure 5. This flow pattern is reminiscent of that induced between two concentric spheres, by rotation of the outer sphere (Greenspan 1968).

We shall denote the characteristic recirculating velocity in the core by u_{c}, and the characteristic (poloidal) boundary velocity by u_{b}. Continuity of mass requires that these velocities are related by

$$u_{\mathrm{b}}\,\delta \sim u_{\mathrm{c}} R_0. \tag{15}$$

One of the conceptual difficulties which arises with this type of flow is the following. In the core, the azimuthal vorticity is of the order of $\omega_{\theta\mathrm{c}} \sim u_{\mathrm{c}}/R_0$, while in the boundary layer, the vorticity is of the order of $\omega_{\theta\mathrm{b}} \sim u_{\mathrm{b}}/\delta$. From (15), we can deduce that

$$\omega_{\theta\mathrm{c}}/\omega_{\theta\mathrm{b}} \sim (\delta/R_0)^2.$$

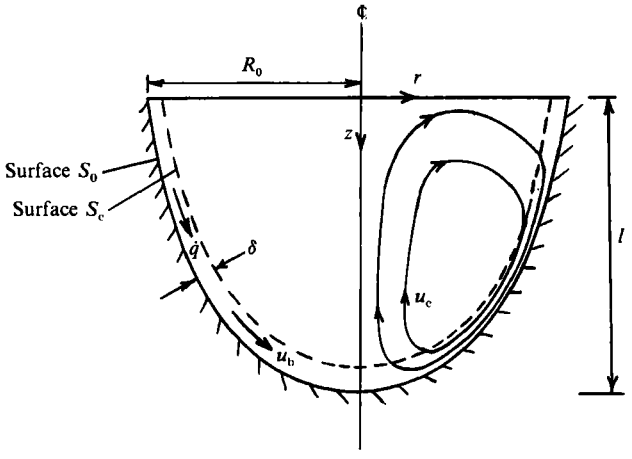

FIGURE 5. Secondary flow for forced swirl in a cavity.

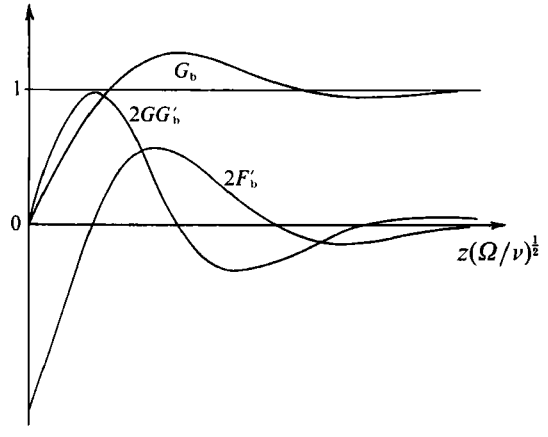

FIGURE 6. Bödewadt's solution for a rotating flow over a stationary disc.

However, as the flow emerges from the boundary layer, we might expect that the boundary vorticity will be carried with the fluid into the core. But this is clearly incompatible with the above scaling. To resolve this dilemma, we must re-examine the exact laminar solution given in the previous section. For laminar flow, the transport equations for angular momentum, $\Gamma = u_\theta r$, and azimuthal vorticity are

$$\boldsymbol{u}\cdot\nabla\Gamma = \nu\left\{\nabla^2\Gamma - \frac{2}{r}\frac{\partial\Gamma}{\partial r}\right\} + \frac{r}{\rho}F_\theta, \tag{16}$$

$$\boldsymbol{u}\cdot\nabla\left(\frac{\omega_\theta}{r}\right) = \nu\left\{\nabla^2\left(\frac{\omega_\theta}{r}\right) + \frac{2}{r}\frac{\partial}{\partial r}\left(\frac{\omega_\theta}{r}\right)\right\} + \frac{\partial}{\partial z}\left(\frac{\Gamma^2}{r^4}\right). \tag{17}$$

The first two terms in (17) represent the familiar advection–diffusion processes. The last term is a source (or flux) of azimuthal vorticity, and arises from the spiralling of the poloidal vortex lines by the azimuthal velocity (Davidson 1989). If we now examine Bödewadt's solution for the boundary layer on the disc, it will become clear what is happening.

Figure 6 shows some relevant aspects of Bödewadt's solution. One of the most striking features of this flow is that u_θ, indicated by the curve G_b, undergoes an

overshoot, followed by oscillations. This is the key to resolving the dilemma. The source term in (17) is proportional to $2G_b G'_b$, and this is also shown in figure 6. Because of the overshoot in u_θ, the source term has both positive and negative regions. The azimuthal vorticity, ω_θ, is proportional to F'_b. Near the wall it is negative. This is a consequence of the no-slip condition, requiring the velocity in the wall jet to fall to zero. Further from the wall, the vorticity is positive.

Now consider a fluid particle which starts near the disc surface, and subsequently migrates up and out of the boundary layer, into the core. Its azimuthal vorticity is governed by (17), which, in this context, simplifies to

$$u_z \frac{\partial}{\partial z}\left(\frac{\omega_\theta}{r}\right) = \nu \frac{\partial^2}{\partial z^2}\left(\frac{\omega_\theta}{r}\right) + \frac{\partial}{\partial z}\left(\frac{\Gamma^2}{r^4}\right).$$

Initially, the particle's vorticity is negative, as a result of its proximity to the wall. As it drifts upward, it picks up positive vorticity from the source term, $2G_b G'_b$. This source term is the primary driving force for the boundary layer, and so the vorticity eventually changes sign, becoming positive. The reason that this vorticity is not then carried out of the boundary layer is that, before leaving, the particle must pass through the outer 'blanket' region, where the source term is negative. In doing so, it loses (nearly) all of its vorticity. It is implicit in figure 5 that a similar process is occurring in the boundary layer on the cavity wall.

We now consider the consequences of the conservation of angular momentum. If we integrate the azimuthal component of the Navier–Stokes equation over an axisymmetric volume V, with bounding surface S, we obtain,

$$\oint_S (\rho\Gamma)\boldsymbol{u}\cdot \mathrm{d}\boldsymbol{S} = \int_V (F_\theta r)\,\mathrm{d}V + \oint_S r\tau_{\theta n}\cdot \mathrm{d}\boldsymbol{S}, \tag{18}$$

where $\tau_{\theta n}$ is the azimuthal surface shear stress. Let S_c be the surface which surrounds the core, but excludes the boundary layer, and S_0 be the cavity surface. Similarly, let V_c and V_0 be the enclosed volumes (see figure 5). Since $\delta \ll R_0$, the volume integral of the body force over volume V_c is essentially the same as that over V_0. Equation (18) applied to the core then gives

$$\oint_{S_c} (\rho\Gamma)\boldsymbol{u}\cdot \mathrm{d}\boldsymbol{S} = \int_{V_0} (F_\theta r)\,\mathrm{d}V.$$

Similarly, the volume integral of the body force over the boundary-layer region, $V_b = V_0 - V_c$, is negligible by comparison with the angular momentum flux across S_c. Consequently, (18) applied to the boundary layer gives

$$-\oint_{S_c} \rho\Gamma\boldsymbol{u}\cdot \mathrm{d}\boldsymbol{S} = \oint_{S_0} r\tau_{\theta n}\cdot \mathrm{d}\boldsymbol{S}.$$

Combining these expressions gives the global angular momentum balance

$$\int_{V_0} (F_\theta r)\,\mathrm{d}V = \oint_{S_c} (\rho\Gamma)\boldsymbol{u}\cdot \mathrm{d}\boldsymbol{S} = -\oint_{S_0} r\tau_{\theta n}\cdot \mathrm{d}\boldsymbol{S}. \tag{19}$$

Equation (19) may be used to give a weighted average of the angular momentum over the boundary S_0. Substituting for F_θ, and using the curvilinear coordinate s, we have

$$\int_0^\delta r^2 \frac{|\tau_{\theta n}|}{\rho}\,\mathrm{d}s = \frac{\Omega_f^2}{4\pi}\int_{V_0} r^2\,\mathrm{d}V, \tag{20}$$

where $\hat{s}$ is the maximum value of s. For turbulent flow, over a smooth surface, the seventh-power-law fit to the law of the wall gives the following well known result for the wall shear:

$$\tau_w = 0.0225\rho u^2(\nu/u\delta)^{\frac{1}{4}}. \tag{21}$$

Following Greenspan (1968), we might apply this equation to swirling flow by taking u to be u_θ at S_c. Substituting into (20) gives

$$0.0225\int_0^{\hat{s}} \Gamma^2 Re_\delta^{-\frac{1}{4}}\,\mathrm{d}s = \frac{\Omega_f^2}{4\pi}\int_{V_0} r^2\,\mathrm{d}V. \tag{22}$$

We shall see later how to estimate $Re_\delta = \Gamma\delta/\nu r$, so that (22) may be used to give an average value of Γ^2 over the surface. It is clear from this equation that the global balance between the surface shear and the Lorentz body force fixes a (weighted) average value for Γ over the surface. The role of inertial forces, such as the Coriolis force, is to determine the distribution of Γ about this mean.

Before looking at the local dynamics of the flow, it is useful to consider one more global balance. Let us define the (volumetric) mass flux in the boundary layer as $\dot{q}$. If u_s is the tangential component of velocity in the boundary layer, and n the distance from the surface, then

$$\frac{\dot{q}}{2\pi r_s} = \int_0^\delta u_s\,\mathrm{d}n.$$

Continuity then requires that, at any given depth z_s

$$\frac{\dot{q}}{2\pi} = -\int_{0_{\text{core}}}^{r_s} (u_z r)\,\mathrm{d}r. \tag{23}$$

In §6, we will see how to calculate the velocity field in the core, so that (23) can then be used to evaluate the mass flux in the boundary layer.

5. Scaling of the velocity field

Let τ_{ns} be the boundary shear stress in the direction of the curvilinear coordinate s, and $\boldsymbol{u}_b$ be the velocity in the boundary layer, comprising of tangential and normal components, u_s and u_n. Then the Navier–Stokes equation, applied to the boundary layer, gives us the following estimates:

$$r,z \quad \text{component:} \quad \boldsymbol{u}_b\cdot\nabla u_s \sim u_\theta^2/r_s \sim |\tau_{ns}|/(\rho\delta),$$
$$\theta \quad \text{component:} \quad \boldsymbol{u}_b\cdot\nabla u_\theta \sim |\tau_{n\theta}|/(\rho\delta).$$

In addition, the azimuthal force balance in the core implies

$$u_c u_\theta \sim \Omega_f^2 r^2.$$

Combining these estimates with (15) gives us

$$u_s \sim u_\theta \sim \Omega_f R_0(R_0/\delta)^{\frac{1}{2}} \sim (R_0\tau_{n\theta}/\rho\delta)^{\frac{1}{2}}. \tag{24}$$

We now estimate δ by relating the wall shear stress to the core velocity. When the flow is laminar, $\tau_{n\theta}$ is of the order of $\rho\nu u_\theta/\delta$, and we may eliminate δ to give

$$u_s \sim u_\theta \sim \Omega_f R_0\{\Omega_f R_0^2/\nu\}^{\frac{1}{3}} \quad \text{(laminar)}. \tag{25}$$

When the flow is turbulent, we may estimate $\tau_{n\theta}$ using (21). This implies

$$u_s \sim u_\theta \sim \Omega_f R_0\{\Omega_f R_0^2/\nu\}^{\frac{1}{5}} \quad \text{(turbulent)}. \tag{26}$$

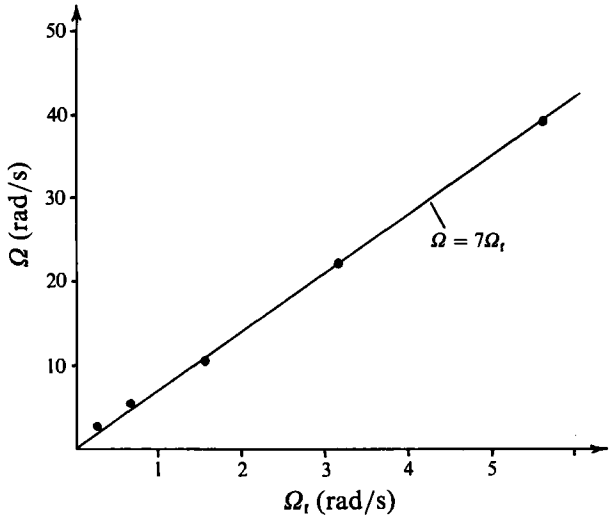

FIGURE 7. Angular velocity measured by Robinson in a truncated cylinder at radius $r = 0.7R_0$.

This result implies that the interaction parameter, N, is small, of the order of $N = \sigma B^2 R_0/\rho u_s \sim Re^{-\frac{1}{2}} u_\theta/\omega R_0$.

Next, we turn our attention to the boundary layer. The ratio of the Lorentz force to the local inertial force is given by (24) as

$$F_\theta r/(\rho \boldsymbol{u}\cdot\nabla\Gamma) \sim \delta/R.$$

It follows that, as in the infinite-disc problem, we may neglect the body force in the boundary layer.

The scaling above should apply equally well to flow in a truncated cylinder, or between parallel discs. Indeed, (25) is consistent with the solution to the disc problem given in §3 (see (14)). Equation (26) was established for flow in a truncated cylinder by Gorbachev & Nikitin (1979), and we shall discuss this in more detail in §10.

Note that (26) predicts an almost linear dependence of u_θ on B. This is precisely what was found by Doronin *et al.* (1973) and Robinson (1973), who independently measured magnetically forced swirl in truncated cylinders. This supports the assertion made in the introduction that, for this class of flow, it is the boundary layers, rather than dissipation in the core, which controls the flow.

In Doronin's experiments, he found that the interior rotation rate, averaged over the inner two-thirds of the cylinder, was proportional to the product of the field frequency and the Hartmann number. The constant of proportionality was 4.3×10^{-3}. Using the present notation, this relationship may be rewritten as $\Omega = 6.7\Omega_f$. The readings were taken in a range of Reynolds numbers of 10^4–10^5. These measurements are consistent with (26).

Robinson's experimental data lie in the range $Re = u_\theta R_0/\nu = 10^6$–$10^7$. His measured core rotation rates near the boundary ($r = 0.7R$) are plotted on figure 7. It can be seen from this figure that the bulk of his data are well approximated by $\Omega = 7\Omega_f$. Again, this is consistent with (26). (Robinson's experiment exhibited some variation of F_θ with z. We have evaluated an effective, or average, Ω_f by integrating his measured distribution of F_θ across the cylinder, both radially and axially.) We shall return to a more detailed discussion of Robinson's data later.

We might contrast (25) and (26) with the equivalent scalings for magnetically forced swirl in an infinitely deep cylinder. As noted in the introduction, this case is

relevant to the magnetic stirring of steel. Davidson (1987) showed that, when the forcing is restricted to a short length of the column, of order R_0, the scaling for both laminar and turbulent flow is, $u_\theta \sim \Omega_f R_0$.

The reason for the different scaling stems from the lack of any Ekman layer in an infinitely deep cylinder. Specifically, the arguments above require that the centripetal and poloidal accelerations are of similar magnitudes in the boundary layer, a condition which is satisfied if an Ekman layer exists. For an infinitely deep column, however, the fluid is free to adopt an axial lengthscale of the order of $1/\nu$, and it is this freedom which allows the global energy balance (1) to be satisfied.

Finally, we note that the estimate of $\tau_{n\theta}$, used to establish these scaling laws, may not be appropriate to the rough dendritic surface encountered during solidification.

6. The interior flow

The fact that the secondary flow in the core is weak has profound implications for the structure of the interior flow. Equation (17), applied to the inviscid core, requires

$$\boldsymbol{u}\cdot\boldsymbol{\nabla}(\omega_\theta/r) = (\partial/\partial z)(\Gamma^2/r^4).$$

This equation holds for both laminar and turbulent flows, but its left-hand-side is of the order of

$$\boldsymbol{u}\cdot\boldsymbol{\nabla}(\omega_\theta/r) \sim u_c^2/R_0^3 \sim u_\theta^2\delta^2/R_0^5.$$

It follows that, in the core, the lengthscale for axial variations in swirl must be of the order of $(R_0/\delta)^2 R_0$. Consequently, the interior swirl flow is of the form

$$\Gamma = \Gamma(r)\{1+0((\delta/R_0)^2)\}. \tag{27}$$

This is reminiscent of the Taylor–Proudman theorem (see Greenspan 1968), the existence of which is usually established on the *a priori* assumption of a vanishingly small recirculation. The angular momentum equation in the core is,

$$\boldsymbol{u}\cdot\boldsymbol{\nabla}\Gamma = F_\theta r/\rho.$$

Since Γ is independent of z, this reduces to

$$u_r\Gamma'(r) = \tfrac{1}{2}\Omega_f^2 r^2, \tag{28}$$

which implies that u_r is also independent of z. The axial velocity component can now be found from the continuity equation,

$$u_z = -(1/r)(\mathrm{d}/\mathrm{d}r)[ru_r]z. \tag{29}$$

Equations (27), (28) and (29) show that the interior flow is uniquely determined by the single unknown function $\Gamma(r)$. In view of (22), we would expect that $\Gamma(r)$ is determined by the boundary-layer equations, and we shall show later that this is indeed the case.

Equation (28) indicates that, in the core, the Lorentz force is balanced exactly by the Coriolis force. The same force balance was evident in the parallel-disc flow, discussed in §3. In addition, both u_r and Γ are independent of z which, again, was a feature of the parallel-infinite-disc flow.

In §4 we introduced the concept of the boundary-layer mass flux, $\dot{q}$. Using (23), we may evaluate $\dot{q}$ from the core flow. The result is

$$\frac{\dot{q}}{2\pi r_s} = \frac{\tfrac{1}{2}\Omega_f^2 z_s r_s^2}{\Gamma_c'(r_s)}, \tag{30}$$

where Γ_c is the core angular velocity at the edge of the boundary layer, $\Gamma_c = \Gamma(r_s)$.

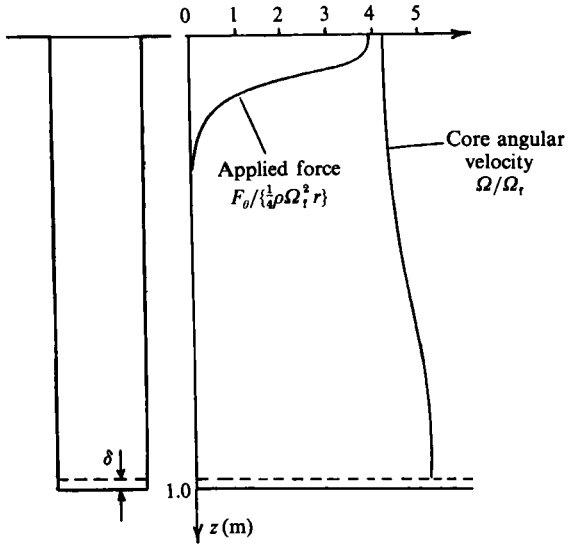

FIGURE 8. Computation of forced swirl in a deep cylindrical cavity.

The derivation of (27) does not depend on the detailed distribution of the body force, and would apply equally well if F_θ varied with z. It is also applicable to flow in a cylindrical cavity. This assertion is supported by the laminar computations of Kapusta & Zibol'd (1982), who investigated forced swirl in a truncated cylinder. It is also in agreement with the experiment of Vives & Perry (1988) and of Robinson (1973). All three found that Γ was independent of z. In the latter case, there was virtually no detectable variation in u_θ with z, despite an axial variation in F_θ of around 50%.

Further support for this hypothesis is given by the following numerical experiment. We have computed the distribution of swirl generated in a cylindrical cavity by a non-uniform body force, F_θ. The flow was taken as turbulent, and the results are shown in figure 8.

The computations were performed using a finite-difference code, employing a power-law differencing scheme and the SIMPLE algorithm. Further details of the numerical scheme may be found in Patankar (1980). The Reynolds stresses are estimated using the standard (k, ϵ)-model, described by Rodi (1984). Since the interaction parameter, N, calculated in §5 is very small (around 0.01), we have made no allowance for the influence of the magnetic field on the turbulence. The body force is that given by (3), but multiplied by a dimensionless, z-dependent function. The axial variation in this force, along with the angular velocity on the axis, is shown in figure 8. The characteristic angular velocity, Ω_f, length, l, and radius, R_0, have values of 10 rad/s, 1 m and 0.1 m respectively.

Despite the fact that the magnetic body force is highly localized, the core angular velocity is surprisingly uniform (to within 18%) along the length of the column. In addition, the secondary flow in the core is small. The peak swirl velocity is 4.5 m/s, while the maximum radial and axial velocities are 0.01 and 0.31 m/s respectively. It is interesting to note that, even in this relatively deep cylinder, the bottom face still restricts the axial lengthscale of the flow.

We shall now examine the boundary-layer equations and show how to determine

Γ. However, it is interesting to note in passing that all five characteristics of the infinite-parallel-disc problem, listed at the end of §3, have manifested themselves in this more general geometry.

7. The momentum integral equations for the boundary layer

Nearly all laboratory experiments and industrial applications of magnetic stirring have Reynolds numbers in excess of 10^4. Consequently, we are interested primarily in turbulent flow. There are two options open to us. Either we can perform a full numerical simulation, perhaps using an eddy-viscosity model, or else we use an approximate technique, such as the momentum-integral method. We shall adopt the second of these approaches, as it lends itself to a more general form of analysis. However, the penalty we pay is a potential loss of accuracy. Consequently, we shall compare our approximate analysis with both physical and numerical experiments in §10.

We shall use the surface arclength, s, and the normal distance from the surface, n, as the local coordinates in the boundary layer. In addition, we shall assume that the surface radius of curvature, R_c, is much greater than δ. Recalling that F_θ may be neglected in the boundary layer, the angular momentum equation is

$$\rho \boldsymbol{u}\cdot\nabla\Gamma = \frac{1}{r}\left\{\frac{\partial}{\partial s}[r^2\tau_{\theta s}] - \frac{\partial}{\partial n}[r^2\tau_{n\theta}]\right\}. \tag{31}$$

If we restrict ourselves to regions where $r_s \gg \delta$, then $\tau_{\theta s}$ is a second-order quantity and may be omitted from (31). The poloidal momentum equation is

$$\rho\left\{\boldsymbol{u}\cdot\nabla u_s + \cos\phi\frac{u_\theta^2}{r}\right\} = \cos\phi\frac{\sigma_{\theta\theta}}{r} + \frac{1}{r}\frac{\partial}{\partial s}[r\sigma_{ss}] + \frac{1}{r}\frac{\partial}{\partial n}[r\tau_{ns}],$$

where $\sigma_{\theta\theta}$ and σ_{ss} are normal stresses. Again, provided we exclude the region near the axis, we may simplify this equation by retaining only the pressure contribution to the normal stresses.

$$\rho\left\{\boldsymbol{u}\cdot\nabla u_s + \cos\phi\frac{u_\theta^2}{r}\right\} = -\frac{\partial p}{\partial s} + \frac{1}{r}\frac{\partial}{\partial n}[r\tau_{ns}]. \tag{32}$$

These equations may be integrated through the boundary layer. Making use of the continuity equation,

$$\nabla\cdot\boldsymbol{u} = \frac{1}{r}\frac{\partial}{\partial s}[ru_s] + \frac{1}{r}\frac{\partial}{\partial n}[ru_n] = 0, \tag{33}$$

the integrated equations of motion may be written in the usual form (see Greenspan 1968)

$$\frac{\mathrm{d}}{\mathrm{d}s}\left\{r_s\int_0^\delta [\Gamma_c - \Gamma]\,u_s\,\mathrm{d}n\right\} - \frac{\dot{q}}{2\pi}\frac{\mathrm{d}\Gamma_c}{\mathrm{d}s} = \frac{r_s^2}{\rho}\tau_\theta, \tag{34}$$

$$\frac{\mathrm{d}}{\mathrm{d}s}\left\{r_s\int_0^\delta u_s^2\,\mathrm{d}n\right\} + \frac{1}{r_s^2}\frac{\mathrm{d}r_s}{\mathrm{d}s}\int_0^\delta [\Gamma_c^2 - \Gamma^2]\,\mathrm{d}n = -\frac{r_s}{\rho}\tau_s. \tag{35}$$

Here τ_θ and τ_s are the boundary shear stresses, taken as positive in the direction of θ and s. Again, these equations are not, in general, valid near the axis.

At this point it is worth considering the consequences of dropping the shear stress $\tau_{\theta s}$ from (34). We have justified this by limiting our solution to $r_s \gg \delta$. Consider now

a region near the axis, where the cavity surface is (almost) flat and horizontal. The neglected term in (34) is

$$\frac{1}{\rho}\frac{\partial}{\partial r}\left\{r^2\int_0^\delta \tau_{r\theta}\,\mathrm{d}z\right\} \sim r^2\nu_t\,\delta\frac{\partial}{\partial r}\left(\frac{u_\theta}{r}\right),$$

where ν_t is an eddy viscosity. This shear stress arises from differential rotation between adjacent cylindrical surfaces within the fluid. It does not rely on the proximity of the boundary, and its magnitude is proportional to the radial gradient in angular velocity. In contrast, the shear stress that we have retained in (34) is

$$(r^2/\rho)\,\tau_{\theta z} \sim \nu_t r^2(u_\theta/\delta).$$

This arises directly from differential rotation between the fluid and the boundary. Clearly, our neglect of $\tau_{r\theta}$ is valid when $r_s \gg \delta$. However, it is precisely this neglected shear stress which, near the axis, guarantees that u_θ varies linearly with r. If we throw out this term, we can no longer ensure that the angular velocity is constant near the axis. Consequently, a solution of the boundary-layer equations (34) and (35) will not, in general, predict $u_\theta \propto r$ as $r \to 0$. Rather, there will be an inner region near the axis where the solution breaks down, and $\tau_{r\theta}$ cuts in to smooth out any potential singularity in u_θ/r. We shall refer to this inner region, of size $r \sim \delta$, as the concentrated viscous core.

Let us now return to our boundary-layer equations. Following the usual procedure, we assume that we can approximate Γ and u_s by

$$\Gamma = \Gamma_c f(n/\delta), \qquad u_s = \hat{u}_s\, g(n/\delta),$$

where $\hat{u}_s$ is a characteristic poloidal velocity in the boundary layer. From these universal profiles, we may deduce

$$\int_0^\delta [\Gamma_c - \Gamma]\,u_s\,\mathrm{d}n = \chi_1\Gamma_c\frac{\dot{q}}{2\pi r_s}, \quad \int_0^\delta u_s^2\,\mathrm{d}n = \chi_2\left(\frac{\dot{q}}{2\pi r_s}\right)^2\delta^{-1}, \quad \int_0^\delta [\Gamma_c^2 - \Gamma^2]\,\mathrm{d}n = \chi_3\Gamma_c^2\,\delta.$$

Here χ_1, χ_2 and χ_3 are constants which may be evaluated from f and g. Of course, there is a certain arbitrariness in the choice of f and g, and so we cannot guarantee that these constants will be accurately established. For turbulent flow, we might follow von Kármán (1921), and take f and g to be given by the seventh-power law,

$$f(\zeta) = \zeta^{\frac{1}{7}}, \quad g(\zeta) = \zeta^{\frac{1}{7}}(1-\zeta).$$

In this case, the constants are

$$\chi_1 = \tfrac{1}{6}, \quad \chi_2 = 1.242, \quad \chi_3 = \tfrac{2}{9}.$$

Clearly, one weakness of the momentum integral approach is the uncertainty in χ_1, χ_2 and χ_3. However, we shall see in §11 that, typically, the predictions of our analysis are insensitive to these constants. Substituting for the integrals in the boundary-layer equations gives

$$\chi_1\frac{\mathrm{d}}{\mathrm{d}s}\left\{\Gamma_c\left[\frac{\dot{q}}{2\pi}\right]\right\} - \frac{\dot{q}}{2\pi}\frac{\mathrm{d}\Gamma_c}{\mathrm{d}s} = \frac{r_s^2\tau_\theta}{\rho}, \tag{36}$$

$$\chi_2\frac{\mathrm{d}}{\mathrm{d}s}\left\{\left[\frac{\dot{q}}{2\pi}\right]^2\frac{1}{r_s\delta}\right\} + \chi_3\frac{\Gamma_c^2\,\delta}{r_s^2}\frac{\mathrm{d}r_s}{\mathrm{d}s} = -\frac{r_s\tau_s}{\rho}. \tag{37}$$

It remains to specify the surface shear stresses. For turbulent flow over a smooth surface, we follow Greenspan and use (21). (Of course, this may not be appropriate

for the dendritic interface in the sump of a caster.) Using this form of the law of the wall, the azimuthal shear stress becomes

$$r_s^2 \tau_\theta/\rho = 0.0225 \Gamma_c^2 Re_\delta^{-\frac{1}{4}}, \tag{38}$$

where, as before, $Re_\delta = \Gamma_c \delta/\nu r_s$. Evaluation of τ_s is slightly more complex. Again, following von Kármán (1921), we might take

$$\tau_s = \frac{\hat{u}_s}{\Gamma_c/r_s}\tau_\theta, \tag{39}$$

which gives us

$$\frac{r\tau_s}{\rho} = 0.0551 \frac{\dot{q}}{2\pi r_s}\frac{\Gamma_c}{\delta} Re_\delta^{-\frac{1}{4}}. \tag{40}$$

Equations (38) and (40) assume implicitly that u_θ is the dominant velocity in the boundary layer. We shall see in §11 that, typically, this is indeed the case.

For laminar flow, one might follow the strategy of von Kármán (1921) and expand f and g as polynomials in n/δ. In any event, we may substitute for the shear stresses in (36) and (37), using either the turbulent relations (38) and (40), or else suitable laminar approximations.

The resulting boundary-layer equations contain only three dependent variables: Γ_c, δ and $\dot{q}$. However, we have already related the boundary-layer mass flux, $\dot{q}$, to Γ_c through the interior flow solution. This relationship is given by (30). Consequently, we have two, coupled, differential equations for Γ_c and δ. For any given surface shape $(r_s(s), z_s(s))$, these may be integrated to furnish $\Gamma_c(r)$. The interior flow solution then follows from (28) and (29).

8. The governing equations for the swirl distribution and boundary-layer thickness

We now eliminate the boundary-layer mass flux from the momentum integral equations. Using (30), we obtain

$$\chi_1 \frac{\mathrm{d}}{\mathrm{d}s}\left\{z_s r_s^3 \frac{\Gamma_c(r_s)}{\Gamma_c(r_s)}\right\} - z_s r_s^3 \frac{\mathrm{d}r_s}{\mathrm{d}s} = \frac{2}{\Omega_f^2}\frac{r_s^2 \tau_\theta}{\rho}, \tag{41}$$

$$\chi_2 \frac{\mathrm{d}}{\mathrm{d}s}\left\{z_s^2 r_s^5 \left[\frac{\Omega_f^2}{2\Gamma(r_s)}\right]^2 \frac{1}{\delta}\right\} + \chi_3 \frac{\Gamma_c^2 \delta}{r_s^2}\frac{\mathrm{d}r_s}{\mathrm{d}s} = -\frac{r_s \tau_s}{\rho}. \tag{42}$$

Note that δ appears in (41) only to the extent that it is required to evaluate Re_δ, and hence τ_θ. If Re_δ were known, then this equation could be integrated to determine $\Gamma_c(r_s)$, without reference to the poloidal equation. Equation (42) therefore takes on the subsidiary role of determining the intermediate variable, δ.

We shall now attribute some physical significance to the terms in (41). If we integrate this equation all the way along the surface, from $s = 0$ to the axis, then the first term integrates to zero and we obtain,

$$\tfrac{1}{2}\Omega_f^2 \int_0^{R_0} z_s r_s^3 \,\mathrm{d}r_s = \int_0^{\hat{s}} \frac{r_s^2 \tau_\theta}{\rho}\mathrm{d}s.$$

However, the left-hand side may be simplified using the relationship,

$$\int_{V_0} r^2 \,\mathrm{d}V = 2\pi \int_0^{R_0} z_s r_s^3 \,\mathrm{d}r_s$$

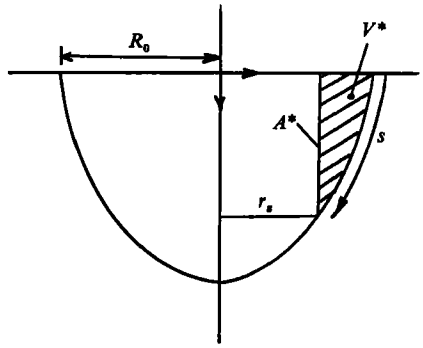

FIGURE 9. Physical interpretation of the azimuthal boundary-layer equation. Equation (44) represents the conservation of angular momentum for the shaded region.

to give
$$\tfrac{1}{2}\Omega_1^2 \int_{V_0} r^2 \,\mathrm{d}V = 2\pi \int_0^s \frac{r_s^2 \tau_\theta}{\rho} \mathrm{d}s. \tag{43}$$

This is simply (20), representing the global balance between the Lorentz force and the surface shear stress. The above integral relationship effectively fixes the (weighted) mean value of Γ_c on the surface. Following the line of argument given in §4, we would then expect the first term on the left-hand side of (41) to determine the distribution of Γ_c about this mean, and to be related to the advection of angular momentum in the core. In fact, it is not difficult to show that (41), integrated from 0 to s, is simply
$$-\int_{A^*} \Gamma \boldsymbol{u} \cdot \mathrm{d}\boldsymbol{A} + \tfrac{1}{2}\Omega_1^2 \int_{V^*} r^2 \,\mathrm{d}V = 2\pi \int_0^s \frac{r_s^2 \tau_\theta}{\rho} \mathrm{d}s, \tag{44}$$
where A^* and V^* are defined in figure 9. Equation (44) therefore represents conservation of angular momentum applied to the shaded region shown in figure 9.

9. A simplified swirl equation for turbulent flow

We shall now focus exclusively on turbulent flows, partly because these are the most important from a practical point of view, and partly because the laminar flow is likely to be unstable for all but low Reynolds numbers. The azimuthal boundary-layer equation is
$$\chi_1 \frac{\mathrm{d}}{\mathrm{d}s}\left\{z_s r_s^3 \frac{\Gamma_c(r_s)}{\Gamma_c(r_s)}\right\} - z_s r_s^3 \frac{\mathrm{d}r_s}{\mathrm{d}s} = \frac{2\kappa}{\Omega_1^2} \Gamma_c^2, \tag{45}$$
where κ is a dimensionless friction coefficient,
$$\kappa = 0.0225(\nu r_s / \Gamma_c \delta)^{\frac{1}{4}} = 0.0225 Re_\delta^{-\frac{1}{4}}.$$
We shall now justify treating this friction coefficient as a constant. Since Γ_c and δ are both functions of s, κ will also vary along the surface. However, in view of the $\frac{1}{4}$-power appearing in the definition of κ, it is certain that the variation in κ will be far less marked than the variation of the quantity it multiplies, Γ_c^2. For example, we would expect that the boundary layer will thicken in the direction of the flow, while Γ_c will decrease with increasing s. In that case, κ will vary with s at a rate somewhat less than $\Gamma_c^{-\frac{1}{4}}$. Consequently, it seems consistent with the level of approximation in this analysis, and in particular with the uncertainty in the magnitude of χ_1, to treat κ as a constant. We propose, therefore, to evaluate κ at $s = 0$, and thereafter treat it as fixed.

We now evaluate κ using (41) and (42) applied at $s = 0$. Let us assume that the surface is vertical at $s = 0$, so that

$$\mathrm{d}r_s/\mathrm{d}s = -\cos\phi = -s/R_c + \ldots,$$
$$\mathrm{d}z_s/\mathrm{d}s = \sin\phi = 1 - s^2/(2R_c^2) + \ldots,$$

where R_c is the radius of curvature of the surface at $s = 0$. Then (45) reduces to

$$\Gamma_c'(r_s) = \frac{\Omega_f^2}{2\kappa}\frac{\chi_1 r_s^3}{\Gamma_c}.$$

If we now substitute this into (42), we find that the initial boundary-layer thickness is

$$\delta/(R_0 R_c)^{\frac{1}{2}} = 3.61\kappa/\chi_1.$$

This expression can then be arranged to give the desired result:

$$\kappa = 0.0372\{R_0/R_c\}^{\frac{1}{10}}\{\Gamma_c/\nu\}_0^{-\frac{1}{5}}\chi_1^{\frac{4}{5}}. \tag{46}$$

Our problem of calculating the swirl distribution has now been reduced to integrating (45). To simplify the algebra in the subsequent sections, it is convenient to introduce the scaled variable

$$U(s) = (2\kappa/lR_0^3\Omega_f^2)\,\Gamma_c^2$$

and the (known) geometric function

$$f(s) = -z_s r_s^3 (\mathrm{d}r_s/\mathrm{d}s) R_0^{-3} l^{-1}.$$

Then the boundary-layer equation may be written in the more compact form

$$-2\chi_1 \frac{\mathrm{d}}{\mathrm{d}s}\left\{f(s)\frac{U(s)}{U'(s)}\right\} + f(s) = U(s). \tag{47}$$

Integration of this second-order equation for a given geometry function is straightforward. We shall consider two specific examples, corresponding to cylindrical and hemispherical geometries.

10. Example 1: swirl in a flat-bottomed cavity

As our first application of the theory, we shall consider the geometry shown in figure 10. The cavity has a flat base and steep sidewalls ($t \ll R_0$). The flow emerges from the bottom boundary layer, picks up angular momentum in the core, and recirculates back via the sides. We shall divide the flow field into three distinct regions: the core, the sidewalls, and the bottom boundary layer. The angular momentum flux (per unit mass) out of each region will be represented by $\dot{\Gamma}_1$, $\dot{\Gamma}_2$, and $\dot{\Gamma}_3$, as shown in figure 10. In addition, we shall denote the net magnetic moment applied to the core by Δ_f,

$$\Delta_f = \int \frac{F_\theta r}{\rho}\,\mathrm{d}V = \tfrac{1}{4}\pi\,\Omega_f^2 R_0^4 l, \tag{48}$$

and the torque exerted by the shear stress on the base and on the sidewalls by

$$T_b = 2\pi\int_0^{R_0}\frac{\tau_\theta r^2}{\rho}\,\mathrm{d}r = 2\pi\kappa\int_0^{R_0}\Gamma_c^2(r)\,\mathrm{d}r, \tag{49}$$

$$T_s = 2\pi\int_0^{l}\frac{\tau_\theta R_0^2}{\rho}\,\mathrm{d}z = 2\pi\kappa l\,\Gamma_c^2(R_0). \tag{50}$$

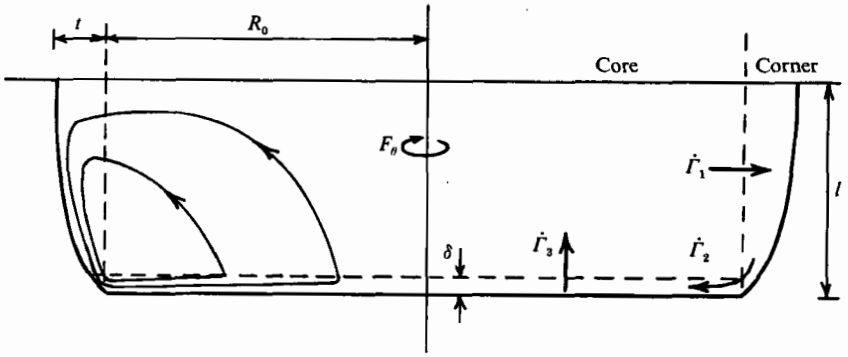

FIGURE 10. Forced swirl in a flat bottomed cavity. $\dot{\Gamma}$ represents the angular momentum flux.

We have already established that the magnetic force may be neglected in the boundary layers. Since we have assumed that the sidewalls are steep, conservation of angular momentum requires that the difference between $\dot{\Gamma}_1$ and $\dot{\Gamma}_2$ must be equal to T_s. Similarly, T_b is equal to the difference in $\dot{\Gamma}_2$ and $\dot{\Gamma}_3$. In fact, all of the quantities defined above may be related to $\dot{\Gamma}_1$ in the following way:

$$\dot{\Gamma}_2 = (1-\chi_1)\dot{\Gamma}_1, \tag{51}$$

$$\dot{\Gamma}_3 = \dot{\Gamma}_1 - \Delta_f, \tag{52}$$

$$T_b = \Delta_f - \chi_1 \dot{\Gamma}_1, \tag{53}$$

$$T_s = \chi_1 \dot{\Gamma}_1. \tag{54}$$

(The first of these equations follows from the definition of χ_1.) These global relationships provide the boundary conditions needed to match the flows in adjacent regions. We shall now determine $\dot{\Gamma}_1$ by application of the boundary-layer equation (47). Applied to the base of the cavity, this equation becomes,

$$-2\chi_1 r^3 \frac{U(r)}{U'(r)} + \tfrac{1}{4}r^4 = R_0^3 \int_0^r U(r)\,\mathrm{d}r. \tag{55}$$

We now introduce the auxiliary function,

$$V(\eta) = \int_0^\eta U(\eta)\,\mathrm{d}\eta, \quad \eta = r/R.$$

In terms of V, our differential equation is

$$V''(\tfrac{1}{4}\eta^4 - V) = 2\chi_1 \eta^3 V'.$$

The solution to this second-order equation, which satisfies $V(0) = 0$ and $V'(0) = 0$, is

$$V = (1-\tfrac{8}{3}\chi_1)\tfrac{1}{4}\eta^4.$$

It follows that U is given by

$$U = (1-\tfrac{8}{3}\chi_1)(r/R_0)^3.$$

However, we have not yet considered the boundary condition at the sidewall, which is furnished by (50) and (54):

$$T_s = 2\pi\kappa l \Gamma_c^2(R_0) = \chi_1 \dot{q}(R_0)\Gamma_c(R_0),$$

and which, when $\dot{q}$ is eliminated, gives

$$2\pi\kappa l \Gamma_c^2(R_0) = \chi_1\{\pi\Omega_f^2 l R_0^3\}\Gamma_c(R_0)/\Gamma_c'(R_0).$$

Physically, this boundary condition ensures that the bottom boundary will accept the fluid emerging from the sidewalls. In terms of U, this boundary condition may be rewritten as

$$lU'(R_0) = 2\chi_1.$$

Our simple cubic expression for U will satisfy this additional boundary condition only if

$$\chi_1 = 3l/(2R_0 + 8l).$$

Consequently, we shall choose χ_1 on this basis. Consider, by way of an example, the case where $l = R_0$. Then we require $\chi_1 = 0.3$, and the distribution for Γ_c becomes

$$\Gamma_c = \frac{\Omega_f l^{\frac{1}{2}}}{(10\kappa)^{\frac{1}{4}}} r^{\frac{3}{2}}.$$

The predicted $r^{\frac{3}{2}}$ dependence for Γ_c seems somewhat counter-intuitive. Certainly, it implies the existence of a concentrated viscous core, where our solution breaks down. However, we shall see later that just such a variation in angular velocity manifests itself in Robinson's (1973) experiments.

Substituting for κ, we find that the peak core angular momentum is given by

$$\hat{\Gamma}_c = 1.98\Omega_f l^{\frac{1}{4}} R_0^{\frac{3}{4}} [\Omega_f l R_0/\nu]^{\frac{1}{6}} [R_c/l]^{\frac{1}{16}}. \tag{56}$$

The dependence of Γ_c on the radius of curvature, R_c, is so slight that we may reasonably neglect the term involving R_c/l. When this is discarded, the scaling in (56) is that established in §5.

The boundary-layer mass flux may now be determined using (30). The flow of angular momentum out of the core is found to be

$$\dot{\Gamma}_1 = 2.66\Delta_f.$$

The remaining angular momentum fluxes, as well as the shear stress integrals, are given by (51)–(54). These yield

$$\dot{\Gamma}_2 = 1.87\Delta_f, \quad \dot{\Gamma}_3 = 1.66\Delta_f, \quad T_b = 0.20\Delta_f, \quad T_s = 0.80\Delta_f.$$

Note that four-fifths of the applied magnetic torque is resisted by the sidewalls, and only one-fifth by the base. Also, the flux of angular momentum out of the interior region is almost three times that generated by F_θ in the core.

Gorbachev & Nikitin (1979) have also analysed forced swirl in a truncated cylinder. Their analysis is based on the flow between infinite, parallel plates, and, like us, they employed a momentum integral approach in conjunction with a seventh-power law. Their estimate of the core rotation rate is

$$\Omega = 8.21\Omega_f [\Omega_f l R/\nu]^{\frac{1}{6}} (R/l)^{-\frac{4}{6}}.$$

Although this scaling is the same as ours, their estimate of the core rotation is substantially higher. Presumably, the discrepancy arises from the way the sidewalls are handled.

If we neglect the surface discontinuity at $(r = R_0, z = l)$, we may compare our prediction of peak swirl, $\hat{\Gamma}_c$, with experimental data taken in a truncated cylinder. Perhaps the most comprehensive measurements were taken by Robinson (1973), who made velocity measurements over a wide range of field strengths, from 20 to 530 Gauss. He used a Pitot tube, a moving vane, and hot-film probes to measure velocity. As a result of the effects of probe drag, there is a variation of $\sim 30\%$ between

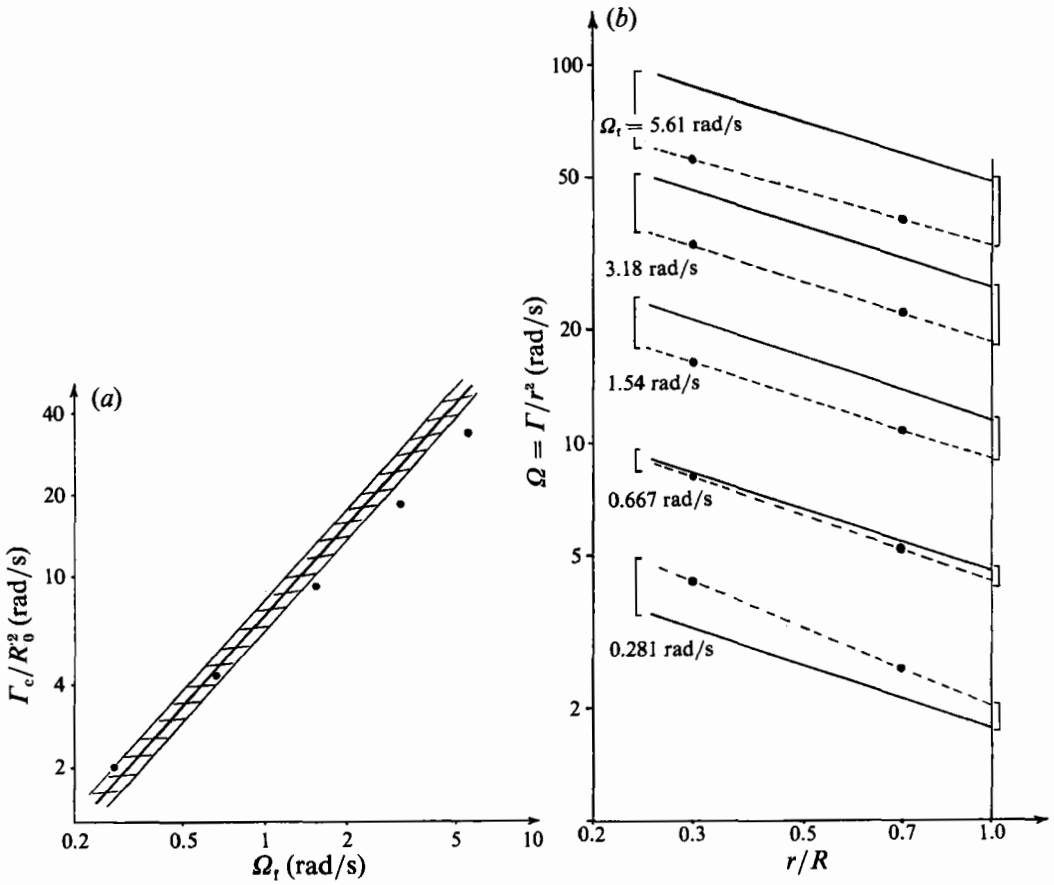

FIGURE 11. Comparison of the theoretical prediction of (*a*) peak swirl (and *b*) angular velocity in a truncated cylinder with the measurements of Robinson (1973): ●, experiment; ——, theory.

measurements taken with different instruments. The most reliable results were obtained using the rotating vane, which was designed specifically to minimize drag on the liquid mercury, and it is these results that we shall consider.

Two difficulties arise in making a direct comparison. They both arise from the fact that we have used an idealized body force, which does not conform to the actual force distribution measured by Robinson. Firstly, there was an axial variation in F_θ of around 50% in Robinson's experiment. To correct for this, we have integrated the measured force distribution throughout the cylinder, and equated this to the magnetic torque induced by our idealized force. This renders an effective, or average, value of Ω_f. However, the force distribution was only measured to within an accuracy of $\pm 25\%$, so that, at best, we can only estimate Ω_f to within $\pm 12\%$. The second difficulty is that there were small components of force F_r and F_z present in the experiment. These could well give rise to a recirculation of similar magnitude to that generated by the boundary layers.

Theory and experiment are compared in figures 11(*a*) and 11(*b*). The first figure shows the variation of peak swirl with forcing, Ω_f. The potential error in our estimate of Ω_f is represented by the shaded region around the theoretical curve. The theory tends to overestimate the swirl at large Ω_f, and underestimate the swirl at low Ω_f. On balance, however, the magnitude is reasonably well predicted. The difference in

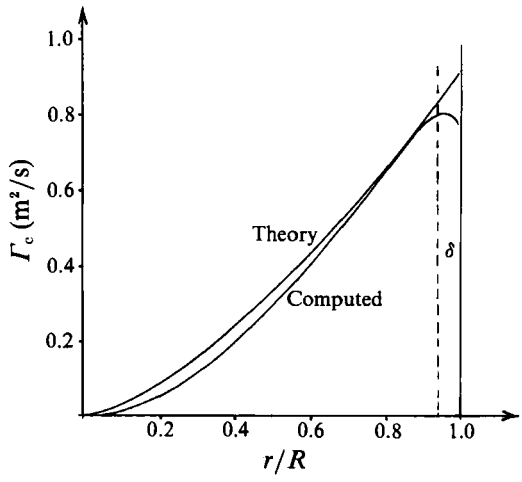

FIGURE 12. Comparison of computed and predicted swirl in a truncated cylinder of unit aspect ratio.

gradient of the two curves is indicative of the fact that Robinson's data more nearly follow a linear relationship between Ω and B, rather than the $\frac{10}{9}$-power law suggested by (56).

Figure 11 (*b*) shows the radial distribution of angular velocity, for a range of values of Ω_f. It is clear that our prediction of

$$u_\theta/r \propto r^{-\frac{1}{2}}$$

also manifests itself in Robinson's data.

Finally, we have performed a full numerical simulation of forced swirl in a truncated cylinder, using the same general purpose (k, ϵ)-model introduced in §6. As with the computation shown in figure 8, we have taken $\Omega_f = 10$ rad/s and $R_0 = 0.1$ m. This time, however, the cylinder is given a half-length of $l = 0.1$ m. Both the computed and predicted distributions for Γ_c are shown in figure 12. The peak swirl seems to be reasonably well predicted, but there is some discrepancy at smaller values of r. This may well be due to the influence of the concentrated viscous core.

11. Example 2: flow in a hemisphere

We now turn our attention to flow in a hemisphere, which, as explained in §1, is of some practical importance in the context of casting.

Let α be the angle between the normal to the boundary and the horizontal. Then we may replace the surface coordinate, s, by $R_0\alpha$, and (47) becomes

$$-2\chi_1 \frac{\mathrm{d}}{\mathrm{d}\alpha}\left\{f(\alpha)\frac{U(\alpha)}{U'(\alpha)}\right\} + f(\alpha) = \mathrm{U}(\alpha), \tag{57}$$

where

$$f(\alpha) = \sin^2\alpha\cos^3\alpha. \tag{58}$$

The global torque balance, (43), requires that

$$\int_0^{\pi/2} U(\alpha)\,\mathrm{d}\alpha = \tfrac{2}{15}. \tag{59}$$

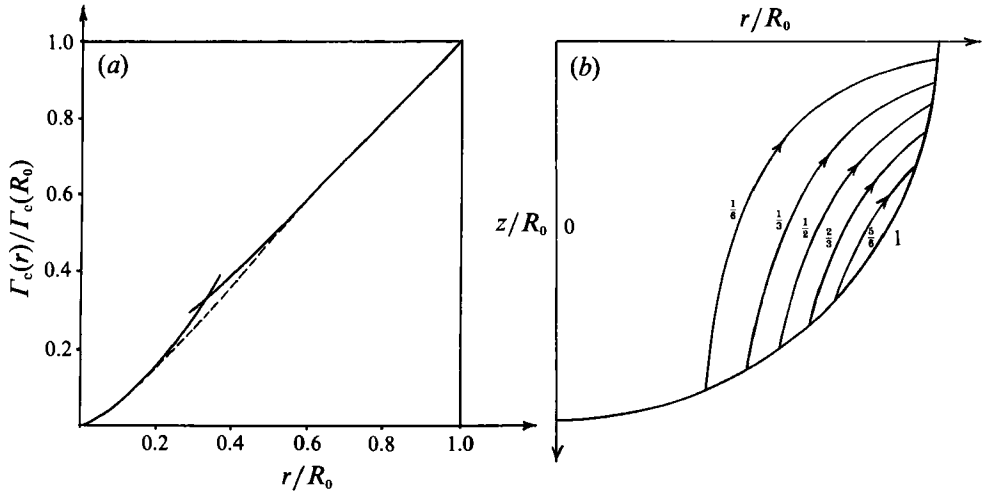

FIGURE 13. (*a*) Matched expansions for Γ_c for forced swirl in a hemisphere. (The exact solution is shown as the dashed line.) (*b*) Secondary flow induced in a hemisphere.

As a prelude to giving an exact solution of (57), we shall find an approximate solution by expanding U about $\alpha = 0$ and $\alpha = \frac{1}{2}\pi$, and then matching the expansions. The expansion about $\alpha = 0$, which satisfies (57) is

$$U_\alpha = m\chi_1 - \chi_1 \alpha^2 + \tfrac{1}{12}\chi_1[11 - 8/m]\alpha^4 + \ldots, \tag{60}$$

where m is a constant to be determined by the matching process.

As suggested in §7, we will take $\chi_1 = \frac{1}{6}$. Then the expansion about $\alpha = \frac{1}{2}\pi$, or $\phi = 0$, which satisfies (57) is

$$U_\phi = \tfrac{5}{9}\phi^3[1 - \tfrac{9}{2}\phi^2 + 25.2\phi^4 + \ldots]. \tag{61}$$

We shall retain only third-order terms in (60) and (61). If we join the two expansions at $\phi = 0.342$, then the global constraint (59) is satisfied, and the gradient of $\Gamma_c(r)$ (or $U^{\frac{1}{2}}(\alpha)$) is reasonably continuous across the join. The matched expansions are shown in figure 13(*a*), in the form of $\Gamma_c(r)$ versus r. The required value of m is 1.02.

A numerical solution of (57) was also obtained as follows. First, we integrate the equation, and then express the result as a second-order equation in $V(\phi)$, the integral of $U(\phi)$. (The definition of V is the same as that used in §10, but with ϕ replacing η.) This new equation can be integrated from $\phi = 0$, subject to $V(0) = 0$ and $V'(0) = 0$. In practice, (61) is used for the initial condition to avoid singular behaviour at the axis. The result is shown on figure 13(*a*), and is similar to the matched expansions.

Note that (61) is, to first order, identical to the expansion of U about $r = 0$ given in the preceeding section. Of course, the r^3 dependence must break down near the axis, where the boundary-layer equations are no longer valid, and a concentrated viscous core appears. From the exact solution of (57), the maximum angular momentum turns out to be

$$\Gamma_c(R_0) = 0.418\,\Omega_f R_0^2/(2\kappa)^{\frac{1}{2}}. \tag{62}$$

Substituting for κ, using (26), yields

$$\Gamma_c(R_0) = 1.96\Omega_f R_0^2[\Omega_f R_0^2/\nu]^{\frac{1}{3}}, \tag{63}$$

which exhibits the expected scaling between Γ_c and Ω_f.

The secondary flow in the core is determined by $\Gamma_c(r)$, through (28) and (29). The

shape of this flow is shown in figure 13(*b*), where equidistant values of the stream function are plotted. The recirculation is largely confined to the outer part of the hemisphere, with the eye of the eddy lying at $\alpha = 35°$.

The mass flux in the boundary layer is determined by (30). This has a maximum value at the eye of the eddy, given by

$$\frac{\dot{q}}{2\pi r_s} = \frac{\Omega_f^2 R_0^4}{3\sqrt{3}\Gamma_c(R_0)}. \tag{64}$$

One concern with the momentum integral approach is the arbitrariness with which χ_1 can be chosen. It is of interest therefore, to determine the sensitivity of the predictions to the magnitude of χ_1. Consequently, we have re-integrated (57) for the value of $\chi_1 = 0.3$. In this case, the peak swirl is predicted to be

$$\Gamma_c(R_0) = 1.98\Omega_f R_0^2 [\Omega_f R_0^2/\nu]^{\frac{1}{6}}. \tag{65}$$

Fortuitously, the difference in predicted swirl is small. For a virtual doubling of χ_1, we obtain only a 1% difference in the predicted value of $\Gamma_c(R_0)$.

12. Analogy to buoyancy-driven flow in a cavity

There is a well-known analogy between swirling flow and thermally driven motion. In both cases, vorticity, ω_θ, can be generated directly in the core of the fluid, thus creating poloidal motion. For a swirling flow, this process is described by (17), and is a result of the swirl velocity spiralling its own vortex lines. For buoyancy-driven flow, the source of vorticity is a radial temperature gradient (Bjerkne's theorem). We shall exploit this similarity to show that many of the features established in §4 have a direct analogy in thermally driven motion. In the interest of simplicity and brevity, we shall restrict ourselves to laminar flow, and only pursue the problem in a qualitative sense.

Consider the steady, axisymmetric flow of liquid metal shown in figure 14. The wall of the cavity is maintained at a reference temperature T_M, while the central part of the upper surface is held at a temperature T_0. The outer, annular region of the top surface is insulated. If T_0 is higher than T_M, then the flow is as shown, falling at the walls and rising up through the core. We shall assume that the core Reynolds number is high. However, we shall take the Prandtl number to be correspondingly small, so that the Péclet number is of order one.

The problem specified above represents a zero-order model of the liquid-metal pool in an aluminium caster. The top surface must be maintained at temperature T_0 by a heat source, and in the case of a caster, this heat is supplied by the incoming melt (whose momentum we ignore). Thermal flows are known to exist in this situation, and these flows have a significant effect on the metallurgical structure of the ingot (Vives & Perry 1988).

We shall assume that density changes are small, and so the velocity field is solenoidal (the Boussinesq approximation). The equation of motion for the fluid is,

$$\mathrm{D}\boldsymbol{u}/\mathrm{D}t = -\boldsymbol{\nabla}(P/\rho) - g\beta(T - T_M)\boldsymbol{k} + \nu\nabla^2\boldsymbol{u} \tag{66}$$

and the corresponding transport equations for vorticity and heat are

$$\frac{\mathrm{D}}{\mathrm{D}t}\left(\frac{\omega_\theta}{r}\right) = \beta g \frac{1}{r}\frac{\partial T}{\partial r} + \nu\left\{\nabla^2\left(\frac{\omega_\theta}{r}\right) + \frac{2}{r}\frac{\partial}{\partial r}\left(\frac{\omega_\theta}{r}\right)\right\}, \tag{67}$$

$$\mathrm{D}T/\mathrm{D}t = \alpha\nabla^2 T. \tag{68}$$

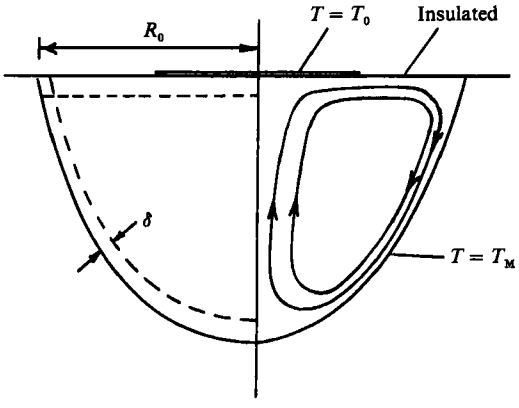

FIGURE 14. Thermally driven flow in a cavity. The upper surface is maintained at temperature T_0, and the walls at the lower temperature of T_M. Cold fluid falls near the walls.

Here α is the thermal diffusivity and β is the expansion constant,

$$\beta = -(1/\rho)(\partial\rho/\partial T).$$

There is an analogy between (67) and (17), with the radial temperature gradient playing the role previously adopted by the axial gradient in angular momentum. Consequently, we might anticipate that, by analogy with (27), the core will be thermally stratified, with the core temperature, T_c, given by

$$T_c \approx T_c(z). \tag{69}$$

That this is so has been shown for certain geometries by the method of matched asymptotic expansions (Yang 1987). However, we shall show here that the same conclusion can be reached more concisely by the method established in §4 for swirl flows. Following the logic of §4, we integrate (66) around a closed streamline to give

$$g\beta\oint(T-T_M)\,dz = \nu\oint\nabla^2\boldsymbol{u}\cdot d\boldsymbol{r}. \tag{70}$$

In view of the assumed smallness of ν, there are three possibilities: (*a*) all the streamlines pass through a boundary layer; (*b*) the core is thermally stratified in accordance with (69); (*c*) the core is isothermal. The last of these options is in accordance with Batchelor's theorem of high-Reynolds-number closed-streamline flows. (In essence, slow diffusion of heat between streamlines homogenizes the temperature.) We shall exclude this possibility for the moment, and concentrate on options (*a*) and (*b*).

It is straightforward to show that if either one of (*a*) or (*b*) holds, then the other must follow. The proof is as follows. Suppose (*b*) holds but (*a*) does not. Then (68) requires

$$u_z T'(z) = \alpha T''(z), \tag{71}$$

which, by virtue of the sloping boundary, requires that (*a*) must hold after all. We may also show that the converse is true by applying the scaling arguments of §5. For convenience, we shall take the datum for the core temperature as T_M. If l is a characteristic axial lengthscale in the core, then the boundary-layer version of (66) requires

$$u_b^2/l \sim g\beta T_c.$$

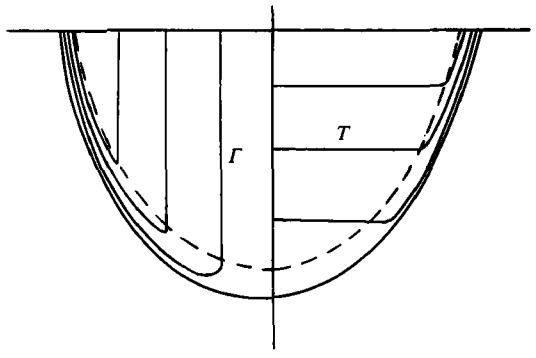

FIGURE 15. A comparison of the isotherms for thermally induced flow with the constant-angular-momentum lines of forced swirl.

In addition, if all the streamlines pass through the boundary layer, continuity gives us

$$u_c \sim u_b \delta/l.$$

These estimates allow the transport of vorticity in the core to be assessed:

$$\boldsymbol{u}\cdot\boldsymbol{\nabla}(\omega_\theta) \sim g\beta T_c \delta^2/l^3,$$

from which, with the aid of (63), we deduce

$$\partial T/\partial r \sim T_c \delta^2/l^3.$$

Consequently, provided the vertical lengthscale, l, is greater than δ, the core is indeed thermally stratified, according to

$$T_c = T_c(z)\{1+O((\delta/l)^2)\}. \tag{72}$$

Thus it appears that either the core must be of the Batchelor-type or else it satisfies both conditions (*a*) and (*b*). A review of the experimental data for confined convection suggests that often the core is indeed stratified, rather than isothermal. This is shown most strikingly in the experiments of Elder (1965), who investigated flow in a two-dimensional slot driven by a temperature difference between the sidewalls. For a high Rayleigh number, the flow is characterized by a combination of a stratified core and thermal wall jets. Elder's experiments were carried out for a high Prandtl number. We are concerned with liquid metal flows where the Prandtl number is low. Yet it appears that a similar behaviour can occur there. Vives & Perry (1988) looked at natural convection in a cylindrical annulus during solidification and, again, a thermally stratified core was found. The same core behaviour manifested itself in the numerical experiments of Flood *et al.* (1989), who looked at flow in the liquid pool of a caster.

We might speculate, then, that the flow shown in figure 14 will be characterized by a quiescent, stratified core, and by thermal wall jets, within which the temperature adjusts from the core distribution to the wall temperature. The analogy between thermal stratification and swirling flow is emphasized in figure 15, where isotherms are compared with the constant-Γ lines of § 11. The role of the thermal jets is to carry hot fluid away from the top surface, and allow it to cool on the cold, curved boundary. In the core, there is a competition between conduction of heat and a weak uniform updraught of cool fluid.

Analytical solutions for thermal wall jets on an inclined surface are well known

(see, for example, Prandtl 1952), and their analogy to Ekman layers is well established (Turner 1973). We might note that Prandtl's solution for a thermal wall jet exhibits the same overshoot in temperature as Bödewadt's solution shows in the Γ-profile.

The idea of a thermally stratified core seems to have come first from Gill (1966), who, following Elder's experiments, analysed high-Reynolds-number flow in a slot. Gill used the method of matched asymptotic expansions, and showed that in the core $T = T(z)$. Moreover, for Prandtl numbers of order one or greater, where conduction in the core may be neglected, he showed that the core velocity was purely horizontal. In this analysis his thermal jets both eject and entrain fluid in such a way that one jet feeds the other via the core. The process is reminiscent of matching the Ekman pumping between parallel discs rotating at different speeds.

Returning to the flow depicted in figure 14, we shall now sketch out how the velocity and temperature fields may be calculated, albeit approximately. Our motivation for doing this is largely to show that the procedure is the same as for the swirling flow problem, thus reinforcing the analogy. Firstly, we use (71) to determine the boundary-layer mass flux:

$$\dot{q} = -\alpha\pi r_s^2 T_c''(z)/T_c'(z).$$

Next, we integrate (66) and (68) across the thermal boundary layer, whose thickness is designated by δ. This gives results analogous to (34) and (35):

$$-\frac{\mathrm{d}}{\mathrm{d}s}\left\{r_s\int_0^\delta u_s(T_c - T)\,\mathrm{d}n\right\} + r_s\int_0^\delta u_s\,\mathrm{d}n\frac{\mathrm{d}T_c}{\mathrm{d}s} = r_s\alpha\left[\frac{\partial T}{\partial n}\right]_0^\delta,$$

$$\frac{\mathrm{d}}{\mathrm{d}s}\left\{r_s\int_0^\delta u_s^2\,\mathrm{d}n\right\} = g\beta r_s\sin\phi\int_0^\delta (T_c - T)\,\mathrm{d}n.$$

We now introduce the (constant) parameters, χ_4 and χ_5, defined in precisely the same way as χ_1 and χ_3, but with T replacing Γ or Γ^2, as appropriate. We can then substitute for the boundary-layer mass flux, to give

$$\frac{\mathrm{d}}{\mathrm{d}s}\left\{r_s^2 T_c'(z) - \chi_4 r_s^2\frac{T_c T_c''(z)}{T_c'(z)}\right\} = 2r_s\left(\frac{\partial T}{\partial n}\right)_0, \tag{73}$$

$$\frac{\mathrm{d}}{\mathrm{d}s}\left\{\frac{r_s^3}{\delta}\left[\frac{T_c''(z)}{T_c'(z)}\right]^2\right\} = \frac{4\chi_5}{\chi_2}\frac{g\beta T_c}{\alpha^2}r_s\,\delta\sin\phi. \tag{74}$$

These equations may be integrated for $T_c(z)$ and $\delta(z)$ for any given shape of cavity. The magnitude of the velocity in the thermal wall jet is of the order of

$$u_b^2 \sim g\beta T_c\, l.$$

For the casting of aluminium, typical parameter values give a boundary-layer velocity of ~ 0.1 m/s. We might compare this estimate with the velocity induced by a rotating magnetic field. Suppose we have a magnetic field of 50 Gauss at a frequency of 1 Hz. Then from (4), (63) and (64), we find that $u_\theta \sim 0.5$ m/s and $u_b \sim 0.1$ m/s. Therefore, in this example, the boundary-layer flows induced by buoyancy and magnetic stirring are similar in magnitude, and in the same direction. Clearly, one of the effects of rotary magnetic stirring in a caster is to augment the thermally induced flow near the boundary. We might speculate, therefore, that the influence of magnetic stirring on the as-cast structure of the ingot will be similar to that of buoyancy.

13. Conclusions

There is a considerable amount of direct and indirect evidence to support the flow structure proposed in §§5 and 6. The z-independence of the core swirl is most dramatically illustrated by the numerical experiment of §6, and is evident in Robinson's data. The scaling laws established in §5 are consistent with the results of Doronin *et al.* and Robinson, and coincide with the exact analysis given in §3 for parallel-disc flow.

The main difficulty arises in handling the boundary-layer equations. We have resorted to a momentum-integral approach, as it allows us some generality in the development of the analysis. Another simplification arises from treating the friction coefficient, κ, as constant, justified by the (asserted) weak dependence of κ on position.

The end product of this analysis is (47), which may be integrated to give the swirl distribution in an axisymmetric cavity of arbitrary profile. This simple second-order ordinary differential equation has considerable generality, but has embedded in it the approximations outlined above. Consequently, its utility can only be established by comparing its predictions with experimental data. One such comparison is made in §10, where our governing equation is applied to flow in a flat-bottomed cavity, and the predictions compared with Robinson's experimental data. Unfortunately, we can find no experimental data with which to compare the analysis of §11, for flow in a hemisphere.

The extension of these ideas from swirling flow to thermal convection is a natural one. However, we have only pursued this in a qualitative sense, establishing the existence of a stratified core (as Gill predicted), and sketching out a procedure for calculating the flow.

I would like to thank Dr F. Boysan for his assistance with the numerical computations. The code used was FLUENT, made available by FLUENT Europe.

REFERENCES

BOYAREVICH, V. & MILLERE, R. 1982 Amplification of azimuthal rotation in a meridional electric vortex flow in a hemisphere. *Magnetohydrodyn.* **18**, 373.

DAHLBERG, E. 1972 On the action of a rotating magnetic field on a conducting liquid. *AB Atomenergi Rep* AE-447. Sweden.

DAVIDSON, P. A. 1989 The interaction between swirling and recirculating velocity components in unsteady, inviscid flow. *J. Fluid Mech.* **209**, 35–55.

DAVIDSON, P. A. & HUNT, J. C. R. 1987 Swirling, recirculating flow in a liquid metal column generated by a rotating magnetic field. *J. Fluid Mech.* **185**, 67–106.

DORONIN, V. I., DREMOV, V. V. & KAPUSTA, A. B. 1973 Measurements of the characteristics of the magnetohydrodynamic flow of mercury in a closed cylindrical vessel. *Magnetohydrodyn.* **9**, 138–140.

ELDER, J. W. 1965 Laminar free convection in a vertical slot. *J. Fluid Mech.* **23**, 77–97.

FLOOD, S. C., KATGERMAN, L., LANGILLE, A. H., ROGERS, S. & READ, C. M. 1989 *Light Metals 1989*, 943–947.

GILL, A. E. 1966 The boundary layer regime for convection in a rectangular cavity. *J. Fluid Mech.* **26**, 515–536.

GORBACHEV, L. P. & NIKITIN, N. V. 1973 Motion of an electrically conducting liquid between two discs in crossed electric and magnetic fields. *Magnetohydrodyn.* **9**, 133–136.

GORBACHEV, L. P. & NIKITIN, N. V. 1979 MHD flow in a cylindrical vessel of finite dimensions with turbulent boundary layers. *Magnetohydrodyn.* **15**, 63–68.

GREENSPAN, H. P. 1968 *The Theory of Rotating Fluids*. Cambridge University Press.

KÁRMÁN, VON T. 1921 Uber laminare und turbulente reibung. *Z. Angew. Math. Mech.* **1**, 233–252.

KAPUSTA, A. B. & ZIBOL'D, A. F. 1982 Three-dimensional effects generated in a finite-length container under the action of a rotating magnetic field. *Magnetohydrodyn.* **18**, 57–63.

MESTEL, A. J. 1989 An iterative method for high-Reynolds-number flows with closed streamlines. *J. Fluid Mech.* **200**, 1–18.

MUIZHNIEKS, A. R. & YAKOVICH, A. T. 1988 Numerical study of closed axisymmetric MHD rotation in an axial magnetic field with mechanical interaction of azimuthal and meridional flows. *Magnetohydrodyn.* **24**, 50–55.

PATANKAR, S. V. 1980 *Numerical Heat Transfer and Fluid Flow*. Hemisphere.

PEDLOSKY, J. 1979 *Geophysical Fluid Dynamics*. Springer.

PRANDTL, L. 1952 *Essentials of Fluid Mechanics*. Blackie.

ROBINSON, T. 1973 An experimental investigation of a magnetically driven rotating liquid-metal flow. *J. Fluid Mech.* **60**, 641–664 (with an Appendix by K. Larsson).

RODI, W. 1984 Turbulence models and their applications in hydraulics. *IAHR State-of-the-Art-Paper*, pp. 26–33.

TURNER, J. S. 1973 *Buoyancy Effects in Fluids*. Cambridge University Press.

VIVES, C. & PERRY, C. 1988 Solidification of pure metal in the presence of rotating flows. In *Liquid Metal Flows: Magnetohydrodynamics and Applications* (ed. H. Branover & M. Mond). Progress in Astronautics and Aeronautics, pp. 515–535. AIAA.

VLASYUK, V. K. & SHARAMKIN, V. I. 1987 Effect of vertical magnetic field on heat and mass transfer in a parabolic liquid metal bath. *Magnetohydrodyn.* **23**, 211–216.

YANG, K. T. 1987 Natural convection in enclosures. In *Handbook of Single-Phase Convective Heat Transfer* (ed. S. Kakac, R. K. Shah & W. Aung), p. 13.12. Wiley.

ZIBOL'D, A. F., KAPUSTA, A. B., KESKYULA, V. F., PETROV, G. N. & REMIZOV, O. A. 1986 Hydraulic phenomenon accompanying the growth of single crystals by Czochralski's method. *Magnetohydrodyn.* **22**, 202–209.